Design and Experimental Evaluation of Immersion and Invariance Observer for Low-Cost Attitude-Heading Reference System

Jafar Keighobadi*, Mehran Hosseini-Pishrobat, Javad Faraji and Milad Naseri Langehbiz

Abstract—This paper presents a new immersion and invariance (I&I) observer for inertial microelectromechanical systems (MEMS) sensors-based, low-cost attitude-heading reference systems (AHRSs). Using the I&I methodology, the observer design problem is formulated as finding a dynamics system, called the observer, and a differentiable manifold in the extended state space of the Euler angles-observer dynamics. The manifold is required to be practically stable with respect to the system trajectories. By imposing this requirement, an observer is derived to robustly estimate the Euler angles. To show the efficacy of the I&I observer and to compare its performance with the extended Kalman filter (EKF), rigorous simulations are performed using the raw data of a set of urban vehicular AHRS tests.

Index Terms—Inertial navigation, Microelectromechanical systems, Nonlinear filters, Observers

I. INTRODUCTION

TTITUDE-heading reference systems (AHRSs), which use inertial microelectromechanical systems (MEMS) sensors and magnetometers, provide a low-cost solution to the Schuler tuning in strapdown inertial navigation systems (INSs) [1], [2]. Inertial MEMS sensors, notwithstanding the advantages such as small size, low-cost, and low power consumption, suffer from bias and mechanical-thermal noises, and their performance is sensitive to environmental fluctuations [3]. Moreover, local magnetic fields usually affect magnetometers' outputs. These factors necessitate using an estimation algorithm in an AHRS to properly combine and process the measurements and to provide consistent attitude-heading estimates. In this regard, Kalman filtering-based algorithms, and the extended Kalman filter (EKF) in particular, are the most prevalent estimation methods used in the inertial navigation applications [4], [5]. However, several shortcomings associated with EKF should be considered. Since it is a linearization-based method, its tuning is often difficult and time-consuming, its performance may be deteriorated in the face of severe nonlinearities, and its convergence cannot be

Manuscript received March 3, 2019; revised August 9, 2019; accepted September 11, 2019.

proved in general [6], [7]. Accordingly, various nonlinear and/or enhanced estimation methods have been reported in the literature. The underlying observer design frameworks of these methods are optimal estimation [2], [8], complementary filtering [9], system transformation-based design [10], unit quaternion-based design [7], [11], [12], and Lie groups-based design [13], [14], [15]. In this paper, we study the problem of attitude-heading estimation by applying a new, alternate observer design framework.

Immersion and invariance (I&I) refers to a class of control and observation methods that employ system immersion and manifold invariance to achieve the design objectives. In the context of the control system design, the basic I&I formulation includes finding a target dynamics, establishing an immersion mapping between the plant and the target dynamics, identifying the invariant manifold determined by the immersion, and, finally, stabilizing the invariant manifold [16], [17]. I&I controllers have been proposed and applied in various application such as robot manipulators [17], quadrotor unmanned aerial vehicles [18], switched systems [19], and chaos suppression in atomic force microscopes [20]. In the context of observer design, the I&I methodology amounts to designing a dynamics system, referred as the observer, and an invariant manifold such that, in the state space of the plantobserver, the trajectories converge to this manifold [17], [21]. Upon the convergence, an asymptotic state estimate can be obtained through any diffeomorphism between the manifold and its associated Euclidean space. I&I observers have been studied for various applications including velocity estimation in holonomic/nonholonomic mechanical systems [21], [22], [23], nonlinear vibration [24], leader-follower formation in unicycle robots [25], and systems with time-delayed measurements [26].

The main contribution of this paper is to propose a novel nonlinear observer for AHRS application by using the I&I design framework. The distinctive features and main novelties of the proposed observer lie at the following points: (i) The design and convergence analysis of the observer are performed in a geometric framework. Unlike the existing methods, the dynamics of the observer is not selected a priori, but rather it is derived constructively from a geometric stabilization problem. (ii) The original definition and formulation of I&I observers [17], [21] assumed no disturbances/noises whereas the attitude dynamics in a low-cost AHRS is subject to sensors' bias

J. Keighobadi, M. Hosseini-Pishrobat, and J. Faraji are with the Faculty of Mechanical Engineering, University of Tabriz, Tabriz, 29 Bahman, P.C. 5166614766, Iran (e-mail: Keighobadi@tabrizu.ac.ir, M.Hoseini92@ms.tabrizu.ac.ir, j.faraji@tabrizu.ac.ir).

M. Naseri Langehbiz is with the Politecnico di Milano, Milan, Italy (email: milad.naseri@mail.polimi.it).

^{*}Corresponding author: Jafar Keighobadi, Tel: +98 4133393045

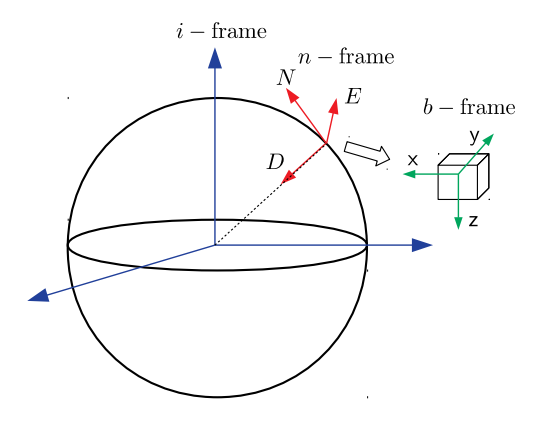


Fig. 1. Schematic of body (b-frame), navigation (n-frame), and inertial (i-frame) reference frames

and noise uncertainties. Hence, we give a new definition of an I&I observer by relaxing the asymptotic convergence to practical convergence. (iii) To handle measurement disturbances, suitable low-pass-filters are incorporated into the observer's dynamics. The observer achieves robustness against input disturbances via a quadratic stabilization-type approach. Moreover, suitable nonlinear gains are used to reach a compromise between the convergence rate and the amplification of the low-pass-filtering errors. Using the data of urban vehicular INS/GPS tests, the performance of the I&I observer is studied by detailed, comparative software simulations, and its accuracy and computational efficiency are investigated.

The rest of the paper is organized as follows. Section II explains the basic mathematical model of an AHRS. Section III elaborates the design and convergence analysis of the proposed I&I observer. Section IV presents the results of comparative software simulations based on a set of vehicular INS/GPS test data. Finally, Section V concludes the paper.

Notation. $\|.\|$ denotes the 2-norm of a vector and $\|.\|_F$ is the Frobenius matrix norm. The operator $\operatorname{sym}(.) := (.) + (.)^\top$ is defined over the square real matrices. The special orthogonal group is given by $\operatorname{SO}(3) := \{X \in \mathbb{R}^{3\times 3} \mid XX^\top = I, \det(X) = 1\}$. The angular velocity vector of a-frame with respect to b-frame, expressed in c-frame, is denoted by ω_{ba}^c .

II. MATHEMATICAL DESCRIPTION OF AHRS

The basic sensor configuration of an AHRS comprises a triaxial inertial measurement unit (IMU), including MEMS gyroscopes and accelerometers, and a triaxial magnetometer; GPS can be also used to provide auxiliary measurements. Consider a vehicle equipped with the AHRS. We define the following right-handed reference frames: (i) b-frame: an x-y-z body frame attached to the vehicle and its axes are aligned with the IMU axes; (ii) n-frame: a local North-East-Down (NED) navigation frame; (iii) i-frame: an Earth-centered inertial frame. Fig. 1 shows a schematic description of these reference frames. The direction cosine matrix (DCM)

 $C_b^n \in SO(3)$, which transforms measurements from the *b*-frame to the *n*-frame, satisfies the kinematic equation

$$\dot{C}_h^n(t) = C_h^n(t)S\left(w_{nh}^b(t)\right),\tag{1}$$

where the skew-symmetric matrix $S\left(w_{nb}^b\right) \in \mathbb{R}^{3\times3}$ is such that the cross product identity $S\left(w_{nb}^b\right)$ (.) = $w_{nb}^b \times$ (.) holds for any vector (.) $\in \mathbb{R}^3$ [4], [27]. One approach to establish a diffeomorphic mapping between the state space of the system (1), SO(3), and a Euclidean space is to use the Euler angles parameterization [27]. Accordingly, by defining ϕ , θ , and ψ as the roll, pitch, and heading angles, respectively, we transform the system (1) into [4]

$$\begin{pmatrix} \dot{\phi}(t) \\ \dot{\theta}(t) \\ \dot{\psi}(t) \end{pmatrix} = G\left(\phi(t), \theta(t), \psi(t)\right) \omega_{nb}^{b}(t), \tag{2}$$

where

$$G(\phi, \theta, \psi) := \begin{pmatrix} 1 & \sin \phi \tan \theta & \cos \phi \tan \theta \\ 0 & \cos \phi & -\sin \phi \\ 0 & \sin \phi \sec \theta & \cos \phi \sec \theta \end{pmatrix}.$$
(3)

For a reliable navigation system, it is imperative to compute the DCM $C_b^n(.)$ consistently and accurately. The biases and noises of the low-cost MEMS gyroscopes render the open-loop integration of the systems (1) or (2) ineffective [1], [10]. Therefore, we design a robust observer using the following AHRS measurements:

Gyroscopes: The output $\omega \in \mathbb{R}^3$ of the IMU gyroscopes is

$$\omega(t) = \omega_{nb}^b(t) + \omega_{in}^b(t) + \delta\omega(t), \tag{4}$$

where $\delta\omega \in \mathbb{R}^3$ accounts for the cumulative effect of the MEMS gyroscopes' bias and noise uncertainties [5], [10].

Accelerometers: Using the output $f := \operatorname{col}(f_x, f_y, f_z) \in \mathbb{R}^3$ of the IMU accelerometers, the roll and pitch angles are calculated, via a vector matching with respect to the Earth's gravity vector, as follows [28]:

$$\phi_c(t) = \operatorname{atan}\left(\frac{-f_{\mathsf{y}}(t)}{-f_{\mathsf{z}}(t)}\right),$$

$$\theta_c(t) = \operatorname{asin}\left(\frac{f_{\mathsf{x}}(t)}{\|f(t)\|}\right),$$
(5)

Magnetometers and GPS: Consider the output vector $m := col(m_x, m_y, m_z) \in \mathbb{R}^3$ of the magnetometers. Through a vector matching with respect to the Earth's magnetic field vector, the magnetic heading is obtained as [1], [10]

$$\psi_{Mag}(t) = a\cos\left(\frac{\bar{m}_1(t)}{\sqrt{\bar{m}_1^2(t) + \bar{m}_2^2(t)}}\right),$$
(6)

where

$$\bar{m}_1 := m_x \cos \theta_c + m_y \sin \phi_c \sin \theta_c + m_z \cos \phi_c \sin \theta_c, \quad (7a)$$

$$\bar{m}_2 := m_y \cos \phi_c - m_z \sin \phi_c. \quad (7b)$$

Additionally, GPS gives a measurement ψ_{GPS} of the true heading. For small vehicle forward velocities, the ground-tracking angles of GPS are not accurate. Hence, to improve

the measurement accuracy, we combine ψ_{Mag} and ψ_{GPS} to calculate the heading as [8]

$$\psi_c(t) = \begin{cases} \psi_{Mag}(t), & \text{forward velocity } \leq 3\frac{\text{km}}{\text{h}}, \\ \psi_{GPS}(t), & \text{otherwise.} \end{cases}$$
 (8)

According to the AHRS explained above, by defining $x \coloneqq \operatorname{col}(\phi,\theta,\psi) \in \mathbb{R}^3$ as the state vector, $u \coloneqq \omega_g \in \mathbb{R}^3$ as the input vector, $\delta u \coloneqq -\omega_{in}^b - \delta \omega \in \mathbb{R}^3$ as the input disturbance, $y \coloneqq \operatorname{col}(\phi_c,\theta_c,\psi_c) \in \mathbb{R}^3$ as the output vector, and $\vartheta \in \mathbb{R}^3$ as the measurement disturbance, we obtain the following mathematical model:

$$\Sigma_{ahrs} : \begin{cases} \dot{x}(t) = \sum_{i=1}^{3} g_i(x(t)) (u_i(t) + \delta u_i(t)), \\ y(t) = x(t) + \vartheta(t), \end{cases}$$
(9)

with $g_i(.)$ being the i-th column of G(.). In vehicular AHRS applications, the pitch angle is far below the singularity point $|\theta|=90^\circ$ and therefore, the function $g_2(.)$ is well-defined.

Remark 1: The main sources of the measurement disturbance ϑ are twofold: (i) bias and noise uncertainties of the accelerometers and magnetometers, (ii) non-gravitational accelerations and local magnetic disturbances perturbing the vector matching equations (5) and (6), respectively.

Remark 2: The vector u corresponds to the gyroscopes' outputs and therefore, it is reasonable to assume that the input vector of Σ_{ahrs} is bounded as $\|u(t)\| \leq u_0$ for a positive u_0 and all $t \in \mathbb{R}^+$. Similarly, the physical meaning of the input and output disturbances of Σ_{ahrs} implies boundedness of these signals. That is, $\|\delta u(t)\| \leq \delta u_0$ and $\|\vartheta(t)\| \leq \vartheta_0$ for some positives δu_0 , ϑ_0 and for all $t \in \mathbb{R}^+$.

III. I&I OBSERVER DESIGN

To attenuate the effect of high-frequency components of the measurement disturbance, we pass the measurement vector through the following low-pass-filter:

$$\Sigma_{lpf} \colon T\dot{y}_f(t) + y_f(t) = y(t),\tag{10}$$

where $y_f \in \mathbb{R}^3$ is the filtered output and $T \coloneqq \operatorname{diag}(\tau_i)_{i=1}^3 \in \mathbb{R}^{3 \times 3}$ contains the time constants $\tau_i > 0$ of the filter. Consider a system of the form

$$\Sigma_{obs} : \dot{\xi}(t) = \alpha \left(\xi(t), y_f(t), u(t), t \right), \tag{11}$$

where $\xi \in \mathbb{R}^3$ and $\alpha \in \mathcal{C}^1(\mathbb{R}^{10}, \mathbb{R}^3)$ is a function to be designed. Consider the manifold

$$\mathcal{M} := \{ (\xi, x, y_f, t) \in \mathbb{R}^{10} \mid x - \beta(\xi, y_f, t) = 0 \},$$
 (12)

with a design function $\beta \in \mathcal{C}^1(\mathbb{R}^7, \mathbb{R}^3)$. Define

$$z \coloneqq x - \beta\left(\xi, y_f, t\right) \tag{13}$$

as an *off-the-manifold coordinate* for \mathcal{M} [17]; that is, z(t) = 0, for all $t \in \mathbb{R}^+$, if and only if $(\xi(t), x(t), y_f(t), t) \in \mathcal{M}$, for all $t \in \mathbb{R}^+$.

Definition 1 (I&I observer): Σ_{obs} , along with Σ_{lpf} , is an observer for Σ_{ahrs} if there exists a function $\beta \in C^1(\mathbb{R}^7, \mathbb{R}^3)$ such that the manifold \mathcal{M} , defined as (12), satisfies the following property:

There exist $a_0 > 0$ and $b_0 \ge 0$ such that, for all $a \le a_0, b > b_0$: (i) for any initial condition $||z(t_0)|| \le a$ the corresponding trajectory z(t), $t \ge t_0$, remains bounded; (ii) there exists a finite reaching time $t_r > 0$ such that $||z(t)|| \le b$, for all $t \ge t_0 + t_r$; (iii) both (i) and (ii) hold uniformly in t_0 .

Remark 3: The original definition of an I&I observer stipulates that \mathcal{M} should be an invariant and attractive manifold [17], [21]. But, here, we adopt an extension of the notion of practical stabilizability [29], [30] regarding the manifold \mathcal{M} . This allows us to handle the input and measurement disturbances within our observer design framework.

Remark 4: According to Definition 1 and Remark 3, as the system trajectories converge to \mathcal{M} , the estimate $\hat{x} := \beta(\xi, y_f, t)$ converges to x practically.

The time derivative of z is given by

$$\dot{z}(t) = \sum_{i=1}^{3} g_i(x(t)) \left(u_i(t) + \delta u_i(t) \right)
- \frac{\partial \beta}{\partial \xi} \alpha \left(\xi(t), y_f(t), u(t), t \right) - \frac{\partial \beta}{\partial y_f} T^{-1} \left(y(t) - y_f(t) \right) - \frac{\partial \beta}{\partial t}.$$
(14)

Assuming that $\partial \beta/\partial \xi$ is nonsingular, we select the following dynamics for Σ_{obs} :

$$\alpha(\xi, y_f, u, t) = \left(\frac{\partial \beta}{\partial \xi}\right)^{-1} \left(\sum_{i=1}^{3} g_i(\hat{x}) u_i - \frac{\partial \beta}{\partial y_f} T^{-1} (\hat{x} - y_f) - \frac{\partial \beta}{\partial t}\right), \tag{15}$$

where $\hat{x} := \beta(\xi, y_f, t)$. Accordingly, the off-the-manifold dynamics is governed by

$$\dot{z}(t) = -\frac{\partial \beta}{\partial y_f} T^{-1} \left(z(t) + \vartheta(t) \right) + \varpi \left(\xi(t), x(t), y_f(t), u(t), \delta u(t), t \right), \tag{16}$$

where

$$\overline{\omega}(\xi, x, y_f, u, \delta u, t) \coloneqq \sum_{i=1}^{3} (g_i(x)(u_i + \delta u_i) - g_i(\hat{x})u_i).$$
(17)

In order to attain a robust stability for the off-the-manifold dynamics (16), we assume that

H1. There exist a positive definite matrix $P \in \mathbb{R}^{3\times 3}$ and a positive ϵ that satisfy the matrix inequality

$$-\operatorname{sym}\left(P\frac{\partial\beta}{\partial y_f}T^{-1}\right) + \frac{2}{\epsilon}P \le 0. \tag{18}$$

Additionally, to facilitate a regional stability analysis, we make the following assumption.

H2. There exist positive functions $\varpi_1^+ \in \mathcal{C}^0(\mathbb{R}^9, \mathbb{R}^+)$ and $\varpi_2^+ \in \mathcal{C}^0(\mathbb{R}^6, \mathbb{R}^+)$ such that

$$\|\varpi(\xi, x, y_f, u, \delta u, t)\| \le \varpi_1^+(\xi, x, y_f) + \varpi_2^+(u, \delta u),$$
 (19)

for all $(\xi, x, y_f, u, \delta u, t) \in \mathbb{R}^{15} \times \mathbb{R}^+$.

Theorem 1: Consider Σ_{obs} with the dynamics (15) and assume that H1 and H2 hold. Then, Σ_{obs} , along with Σ_{lpf} , is an I&I observer for Σ_{ahrs} .

Proof: Let us assume that $(\xi, x, y_f) \in \Omega$, where $\Omega \subset \mathbb{R}^9$ is a compact set covering the desired range of AHRS operation. By Remark 2 and H2, the continuity of the involved functions implies that there exists a positive constant

$$\varpi_0 \coloneqq \sup_{(\xi, x, y_f) \in \Omega} \varpi_1^+(\xi, x, y_f) + \sup_{\|u\| \le u_0, \|\delta u\| \le \delta u_0} \varpi_2^+(u, \delta u),$$
(20)

such that $\|\varpi(\xi, x, y_f, u, \delta u, t)\| \leq \varpi_0$ for all $(\xi, x, y_f, u, \delta u, t) \in \Omega \times \mathbb{R}^6 \times \mathbb{R}^+$. Consider the candidate Lyapunov function $V(z) \coloneqq z^\top P z$; differentiating V(z) with respect to time and taking H1 into account result in

$$\dot{V}(z(t)) \le -\frac{2}{\epsilon} V(z(t))
+ 2(\varpi_0 + \frac{\mu_0 \vartheta_0}{\epsilon}) \frac{\lambda_{\max}(P)}{\sqrt{\lambda_{\min}(P)}} \sqrt{V(z(t))}, \quad (21)$$

for some positive μ_0 . Accordingly, by using the comparison lemma [30], we obtain the inequality for all $t \ge t_0$, $t_0 \in \mathbb{R}^+$;

$$||z(t)|| \le \left(||z(t_0)|| - (\epsilon \varpi_0 + \mu_0 \vartheta_0) \sqrt{\frac{\lambda_{\max}(P)}{\lambda_{\min}(P)}}\right) \times \sqrt{\frac{\lambda_{\max}(P)}{\lambda_{\min}(P)}} \exp\left(-\frac{t - t_0}{\epsilon}\right) + (\epsilon \varpi_0 + \mu_0 \vartheta_0) \frac{\lambda_{\max}(P)}{\lambda_{\min}(P)}.$$
(22)

Let a_0 be any positive such that the intersection of $\|z\| \le a_0$ with Ω is nonempty and $b_0 := \mu_0 \vartheta_0 \lambda_{\max}(P)/\lambda_{\min}(P)$ be the bound imposed by the measurement noise. Let $b > b_0$ and $a \le a_0$ be positives. According to (22), any trajectory starting in the set $\|z\| \le a$ remains bounded. Next, we show that such a trajectory reaches the ultimate bound b in a finite time. Assume that

$$\epsilon < \epsilon^* := \frac{\lambda_{\min}(P)(b - b_0)}{\lambda_{\max}(P)\varpi_0}.$$
 (23)

Defining the reaching time

$$t_{r} := \epsilon \ln \left(\frac{\sqrt{\frac{\lambda_{\min}(P)}{\lambda_{\max}(P)}} \left| a - \sqrt{\frac{\lambda_{\max}(P)}{\lambda_{\min}(P)}} \left(\epsilon \overline{\omega}_{0} + \mu_{0} \vartheta_{0} \right) \right|}{\overline{\omega}_{0} (\epsilon^{*} - \epsilon)} \right), \tag{24}$$

we have $||z(t)|| \le b$ for all $t \ge t_0 + t_r$. Since the above argument holds for all initial times $t_0 \ge 0$, Σ_{obs} and Σ_{lpf} , with the dynamics (15), satisfy Definition 1.

A. I&I observer with nonlinear gains

Consider y_{fi} , the *i*-the component of y_f , with a desired interval of operation $[c_{i1},c_{i2}]\subset\mathbb{R}$. Assume that the objective is to apply the observer gain $k_{i1}>0$ within $[c_{i1},c_{i2}]$ and $k_{i2}>0$ elsewhere. To this end, we set

$$\frac{\partial \beta_i}{\partial y_{fi}} = \frac{k_{i2} - k_{i1}}{2\tau_i^{-1}} \left(\tanh\left(\frac{y_{fi} - c_{i2}}{\varepsilon_i}\right) - \tanh\left(\frac{y_{fi} - c_{i1}}{\varepsilon_i}\right) \right) + k_{i2}\tau_i, \tag{25}$$

where ε_i is a small positive. To obtain a decentralized observer gain, we also set $\partial \beta_j / \partial y_{fi} = 0$ for $j \neq i$. By integration, we obtain

$$\beta_{i}(\xi, y_{f}) = \Pi_{i}^{\top} \xi + \varepsilon_{i} \frac{k_{i2} - k_{i1}}{2\tau_{i}^{-1}} \ln \left(\frac{\cosh\left(\frac{y_{fi} - c_{i2}}{\varepsilon_{i}}\right)}{\cosh\left(\frac{y_{fi} - c_{i1}}{\varepsilon_{i}}\right)} \right) + k_{i2} \tau_{i} y_{fi}, \tag{26}$$

where $\Pi_i \in \mathbb{R}^3$, i=1,2,3, are linearly independent vectors. To verify that (25) satisfies H1, we use linear matrix inequalities (LMIs). For this, let $a_i(t) \coloneqq (\partial \beta_i(t)/\partial y_{fi})T^{-1}$ and $A(t) \coloneqq (\partial \beta(t)/\partial y_f)T^{-1} = \operatorname{diag}\left(a_i(t)\right)_{i=1}^3$. Accordingly, we have the norm-bounded representation

$$A(t) = A_0 + A_1 N(t), (27)$$

where $A_0 = (1/2) \operatorname{diag} (k_{i1} + k_{i2})_{i=1}^3$, $A_1 = (1/2) \operatorname{diag} (|k_{i1} - k_{i2}|)_{i=1}^3$, and $N^{\top}(t)N(t) - I \leq 0$ for all $t \in \mathbb{R}^+$.

Theorem 2: Consider the nonlinear design (25) and the corresponding norm-bounded model (27). For a given positive ϵ , assume that there exists a positive definite matrix $P \in \mathbb{R}^{3 \times 3}$ satisfying the LMI

$$\begin{bmatrix} -\operatorname{sym}(PA_0) + \frac{2}{\epsilon}P + I & PA_1 \\ A_1^{\top}P & -I \end{bmatrix} \le 0.$$
 (28)

Then, H1 holds with P and ϵ .

Proof: Substituting (27) into (18) and using Young's inequality [3] result in

$$\operatorname{sym}(-P(A_0 + A_1 N(t))) + \frac{2}{\epsilon} P \le -\operatorname{sym}(PA_0) + \frac{2}{\epsilon} P + \mu^{-1} P A_1 A_1^{\top} P + \mu I, \quad (29)$$

for any positive μ . If the right-hand side of the inequality (29) is negative semi-definite, then H1 holds. By Schur's complement and homogeneity, this statement is equivalent to the feasibility of the LMI (28) for P.

IV. SIMULATIONS AND TEST RESULTS

To evaluate the performance of the I&I observer, two vehicular tests were conducted: test no.1 in an urban area, and test no. 2 in the university of Tabriz's campus. During these tests, the vehicle undergoes different maneuver conditions such as zigzag, ramps, fast changes in the attitude, and large variations of the heading angle. The implemented AHRS sensors include an ADIS16407 IMU and an HMC1022 magnetic compass both operating at 50 Hz. Additionally, 1 Hz data of a Garmin 35 GPS receiver is used to modify the magnetic heading according to equation (8). The reference data for the Euler angles are obtained from a Vitans INS/GPS operating in the navigation mode. The test vehicle and sensors' installation are shown in Fig. 2, and the vehicle's trajectories during both tests are depicted in Fig. 3. Table I gives the performance specifications of the inertial and magnetic sensors. The values of the Earth's local gravity and magnetic fields are 9.808 m/s² and $50.90 \mu T$, respectively [10]. To alleviate the adverse effects of



Fig. 2. AHRS and reference INS/GPS hardware installed on the test vehicle

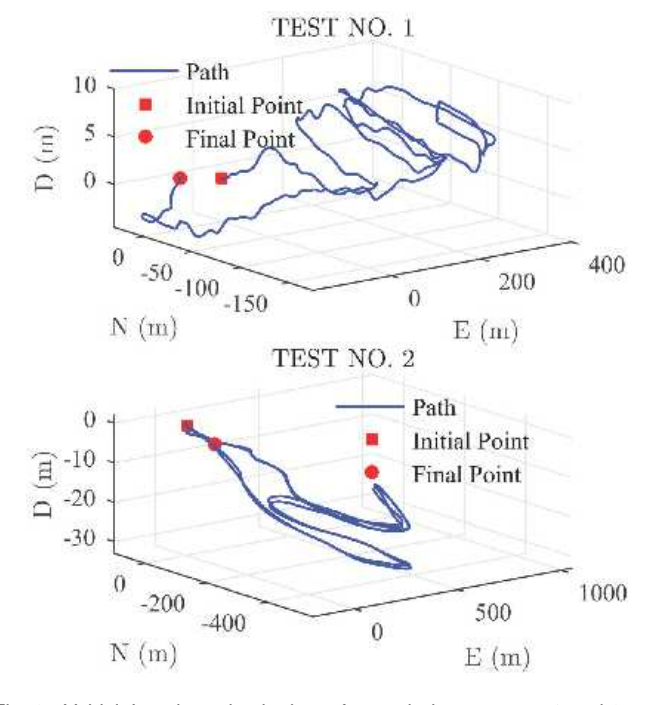


Fig. 3. Vehicle's trajectories in the n-frame during tests no. 1 and 2

local magnetic fields, caused by the vehicle's metallic parts, the magnetic heading is calibrated as follows [31];

$$\psi_{Mag}^{cal} = \psi_{Mag} + \delta \psi_{Mag},$$

$$\delta \psi_{Mag} = a_0^{cal} + \sum_{n=1}^{2} a_n^{cal} \cos(n\psi_{Mag}) + b_n^{cal} \sin(n\psi_{Mag}).$$
(30)

Taking the GPS heading as the reference, the calibration parameters $(a_n^{cal})_{n=0}^2$ (rad) and $(b_n^{cal})_{n=1}^2$ (rad) are obtained, by a least squares optimization [8], as follows:

1) Test no. 1:

$$\begin{aligned} a_0^{cal} &= 0.2942, \ a_1^{cal} = 0.5113, \ a_2^{cal} = -0.0385, \\ b_1^{cal} &= -0.0605, \ b_2^{cal} = 0.3887; \end{aligned}$$

2) Test no. 2:

$$\begin{split} a_0^{cal} &= 0.0169, \ a_1^{cal} = -0.0293, \ a_2^{cal} = -0.0141, \\ b_1^{cal} &= 0.1000, \ b_2^{cal} = -0.0042. \end{split}$$

As a basis for comparison, we design an EKF for Σ_{ahrs} . The parameters of the EKF are tuned as

$$P_{f0} = \operatorname{diag} \left(10^{-5}, 10^{-5}, 10^{-2} \right) \text{ (rad}^{2}),$$

$$Q_{f} = \operatorname{diag} \left(10^{-3}, 10^{-3}, 10^{-1} \right) \text{ (rad}^{2}/\text{s}^{2}), \tag{31}$$

$$R_{f} = \operatorname{diag} \left(1, 1, 0.5 \right) \text{ (rad}^{2}),$$

which correspond to the covariance matrices of initial estimation error, process noise, and measurement noise, respectively; further details can be found in [6], [10]. The parameters of the I&I observer are given in Table II. The gains outside the desired intervals are obtained by solving the linear quadratic regulator (LQR) problem corresponding to the EKF parameters, Q_f and R_f . According to Theorem 2, by performing a bisection search on ϵ , we obtain the optimal values $\epsilon = 31.6250$ and P = diag(15.8197, 15.8197, 2.0306). We also consider the nonlinear attitude/bias observer of Grip et al. [13]. This observer is designed over SO(3) to directly estimate C_h^n along with the gyroscopes' bias vector. We use the accelerometers and magnetometers outputs, in both b- and n-frames, as the vector measurements required by the attitude/bias observer. The differential equations of all observers are implemented in MATLAB R2013b using the Euler's discretization with the sample time of 0.02 s. The raw measurements of the IMU, magnetometers, and GPS are fed to the simulation models. Let $T_{sim} > 0$ be the overall simulation time; we define the following performance indices for comparison of the observers:

1) To measure the convergence time, in terms of the estimation error energy, we define T_{conv} as the smallest time satisfying the energy inequality

$$\int_0^{T_{conv}} ||x(t) - \hat{x}(t)||^2 dt \ge 0.7 \int_0^{T_{sim}} ||x(t) - \hat{x}(t)||^2 dt.$$
(32)

- 2) We measured the execution time, T_{comp} of the main simulation loop for each observer under a 2.70 GHz processor AMD FX-9800P.
- 3) To measure the DCM estimation accuracy, we define an error variable of the form

$$e_{dcm} = \left(\frac{1}{T_{sim}} \int_0^{T_{sim}} \|C_b^n(t) - \hat{C}_b^n(t)\|_F^2 dt\right)^{\frac{1}{2}}.$$
 (33)

The estimation results of the I&I observer, the EKF, and the attitude/bias observer are shown in Figs. 4 and 5, and comparison of the statistical properties (mean value and standard deviation) of the estimation errors are given in Tables III and IV. The comparative data of the performance indices are given in Table V. According to these results, we draw the following conclusions:

 Both I&I and attitude/bias observers outperform the EKF in the roll and pitch estimation channels. In the heading channel, the I&I observer and the EKF have a similar

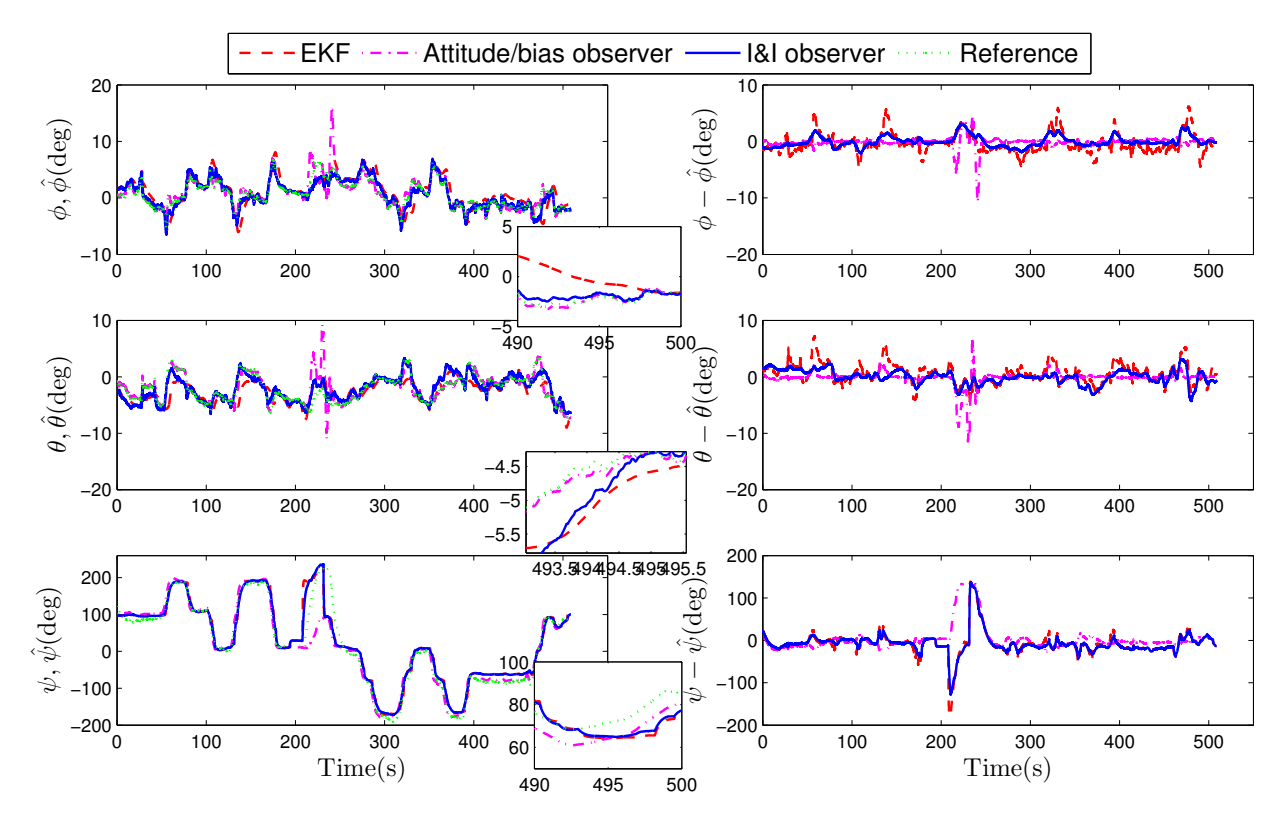


Fig. 4. Estimation results of test no. 1

TABLE I SPECIFICATIONS OF SENSORS

Sensor	Model	FS* range	Noise density	Bias stability	Initial bias error $\pm 1\sigma$	Nonlinearity (%FS)
Gyroscope	ADXRS150	±150°/s	$0.05^{\circ}/\mathrm{s}/\sqrt{\mathrm{Hz}}$	$0.01^{\circ}/{\rm s}$	$\pm 3^{\circ}/\mathrm{s}$	0.1
Accelerometer (single-axis)	ADXL202	$\pm 20 \mathrm{m/s^2}$	$0.01 \rm m/s^2$	$0.05 \rm m/s^2$	$\pm 0.02g$	0.2
Accelerometer (dual-axis)	ADXL210E	$\pm 100 \text{m/s}^2$	0.01m/s^2	$0.05 \rm m/s^2$	$\pm 0.02g$	0.2
Magnetometer	HMC1022	$\pm 200 \mu T^{**}$	$10^{-5} \mu T / \sqrt{Hz}$	$0.10 \mu T$	$2 \times 10^{-5} \mu T$	0.1

^{*}Full-scale

TABLE II
PARAMETERS OF IMMERSION AND INVARIANCE OBSERVER

Estimation channel	Low pass filtering time constant (s)	Desired interval (deg)	Gains and parameters
Roll	$\tau_1 = 0.03$	[-5, 5]	$k_{11} = 5k_{12}, k_{12} = 0.0316, \varepsilon_1 = 1/40, \Pi_1 = [1, 0, 0]^{\top}$
Pitch	$\tau_2 = 0.03$	[-10, 10]	$k_{21} = 5k_{22}, k_{22} = 0.0316, \varepsilon_2 = 1/40, \Pi_2 = [0, 1, 0]^{\top}$
Heading	$\tau_3 = 0.03$	[-100, 100]	$k_{31} = 5k_{32}, k_{32} = 0.4472, \varepsilon_3 = 1/40, \Pi_3 = [0, 0, 1]^{\top}$

TABLE III
STATISTICAL PROPERTIES OF ESTIMATION ERRORS IN TEST NO. 1

Error signal	ror signal I&I observer			EKF	Attitude/bias observer [13]	
	Mean value	Standard deviation	Mean value	Standard deviation	Mean value	Standard deviation
Roll (deg)	0.0294	0.9434	0.3778	1.8041	0.1472	1.0278
Pitch (deg)	0.0275	1.2109	-0.5872	1.7481	0.1727	1.3228
Heading (deg)	7.3541	25.4222	7.7631	28.5094	-3.3008	32.1573

^{**}Micro-Tesla

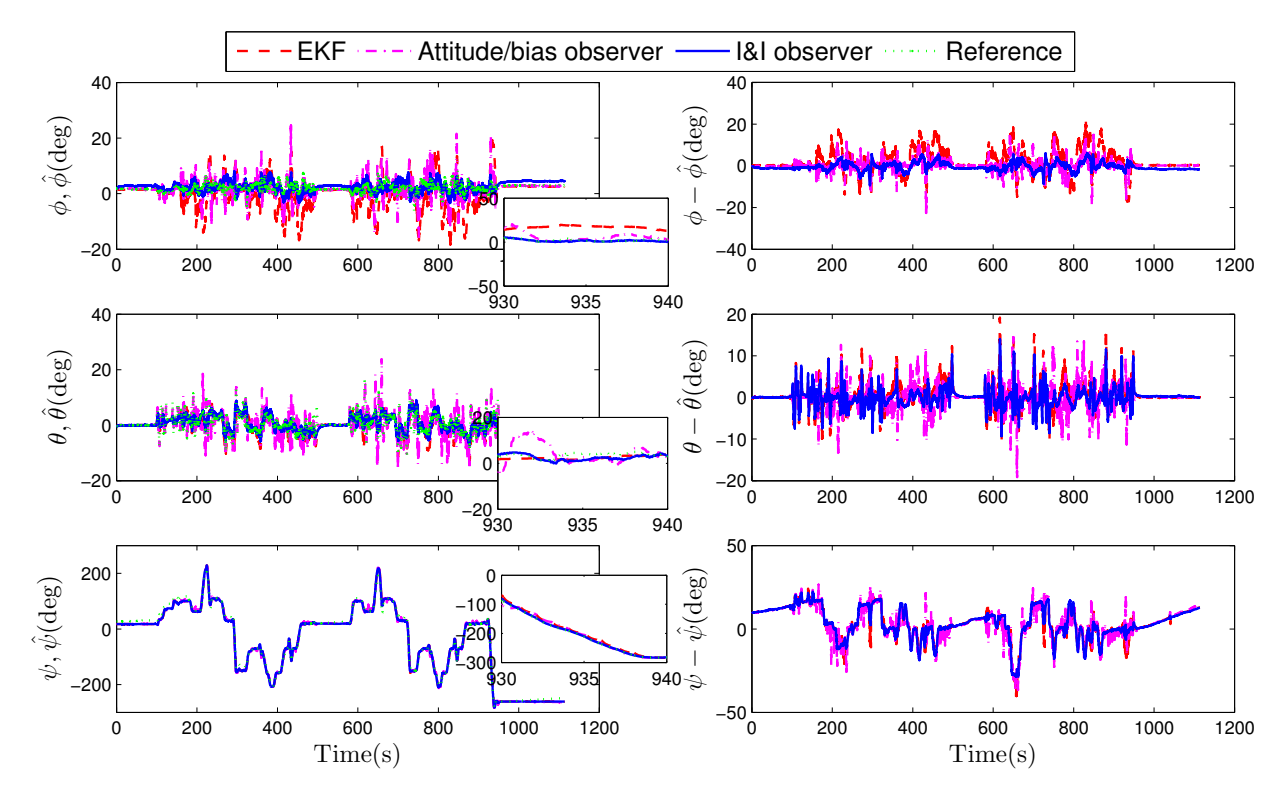


Fig. 5. Estimation results of test no. 2

Error signal	I&I observer			EKF	Attitude/bias observer [13]	
	Mean value	Standard deviation	Mean value	Standard deviation	Mean value	Standard deviation
Roll (deg)	0.5006	1.9231	-2.2319	5.6108	-0.2826	2.8545
Pitch (deg)	-0.0727	2.3138	-0.5821	3.0856	-0.1560	2.5411
Heading (deg)	-3.9367	8.9918	-3.9458	8.9286	-3.6934	9.4267

TABLE V
PERFORMANCE INDICES OF OBSERVERS IN TESTS NO. 1 AND 2

Performance index	I&I observer		EI	ΚF	Attitude/bias observer [13]	
	Test no. 1	Test no. 2	Test no. 1	Test no. 2	Test no. 1	Test no. 2
T_{conv} (s)	239.9600	660.2800	238.2000	696.9000	235.4000	694.2000
T_{comp} (s)	1.3338	2.5409	1.5155	3.4564	8.3097	20.7946
e_{dcm}	0.5840	0.2530	0.6242	0.2917	0.6643	0.2695

performance which, in terms of standard deviation, is better than the attitude/bias observer. However, the heading estimates of the attitude/bias observer have better mean values. Considering the overall estimation accuracy in terms of DCM, the I&I observer yields smaller errors.

• In terms of computational efficiency, the I&I observer outweighs both EKF and attitude/bias observer. The main reasons are 1) the EKF requires recursive linearization of the attitude dynamics and solving a Ricatti equation; 2) the I&I observer works with the three Euler angles parameterization of SO(3) while the attitude/bias observer uses 3×3 DCMs.

V. CONCLUSION

Following a geometric approach, an I&I observer was designed for low-cost AHRS applications. Analytical and numerical analyses were provided to show the effectiveness of the observer. Extending the formulation and the design of I&I observers for the data fusion of an INS/GPS is the future direction of this research.

ACKNOWLEDGMENT

This work was supported by the University of Tabriz's plan to increasing research effectiveness under the contract no. s/858.

REFERENCES

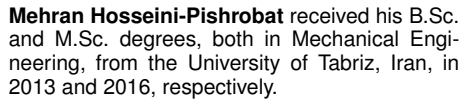
- R. Collinson, Introduction to Avionics Systems, 3rd ed. Dordrecht: Springer Netherlands, 2011.
- [2] J. Keighobadi, M. Yazdanpanah, and M. Kabganian, "An enhanced fuzzy H_{∞} estimator applied to low-cost attitude-heading reference system," *Kybernetes*, vol. 40, DOI 10.1108/03684921111118068, no. 1/2, pp. 300–326, Mar. 2011.
- [3] M. Hosseini-Pishrobat and J. Keighobadi, "Robust output regulation of a triaxial MEMS gyroscope via nonlinear active disturbance rejection," *International Journal of Robust and Nonlinear Control*, vol. 28, DOI 10.1002/rnc.3983, no. 5, pp. 1830–1851, Mar. 2018.
- [4] R. M. Rogers, Applied mathematics in integrated navigation systems, 3rd ed., ser. AIAA education series. Reston, Va: American Institute of Aeronautics and Astronautics, 2007.
- [5] J. L. Crassidis, F. L. Markley, and Y. Cheng, "Survey of Nonlinear Attitude Estimation Methods," *Journal of Guidance, Control, and Dynamics*, vol. 30, DOI 10.2514/1.22452, no. 1, pp. 12–28, Jan. 2007.
- [6] D. Simon, Optimal state estimation Kalman, H infinity and nonlinear approaches. Hoboken, N.J. Wiley-Interscience, 2006.
- [7] P. Martin and E. Salaün, "Design and implementation of a low-cost observer-based attitude and heading reference system," *Control Engineering Practice*, vol. 18, DOI 10.1016/j.conengprac.2010.01.012, no. 7, pp. 712–722, 2010.
- [8] J. Keighobadi, H. Vosoughi, and J. Faraji, "Design and implementation of a model predictive observer for AHRS," GPS Solutions, vol. 22, DOI 10.1007/s10291-017-0696-4, no. 1, p. 854, 2018.
- [9] S. Poddar, P. Narkhede, V. Kumar, and A. Kumar, "PSO Aided Adaptive Complementary Filter for Attitude Estimation," *Journal of Intelligent & Robotic Systems*, vol. 87, DOI 10.1007/s10846-017-0507-8, no. 3-4, pp. 531–543, Sep. 2017.
- [10] P. Doostdar and J. Keighobadi, "Design and implementation of SMO for a nonlinear MIMO AHRS," *Mechanical Systems and Signal Processing*, vol. 32, DOI 10.1016/j.ymssp.2012.02.007, pp. 94–115, 2012.
- [11] H. F. Grip, T. I. Fossen, T. A. Johansen, and A. Saberi, "Non-linear observer for GNSS-aided inertial navigation with quaternion-based attitude estimation," in 2013 American Control Conference, DOI 10.1109/ACC.2013.6579849, pp. 272–279. Washington, DC: IEEE, Jun. 2013.
- [12] T. H. Bryne, J. M. Hansen, R. H. Rogne, N. Sokolova, T. I. Fossen, and T. A. Johansen, "Nonlinear Observers for Integrated INS/GNSS Navigation: Implementation Aspects," *IEEE Control Systems*, vol. 37, DOI 10.1109/MCS.2017.2674458, no. 3, pp. 59–86, Jun. 2017.
- [13] H. F. Grip, T. I. Fossen, T. A. Johansen, and A. Saberi, "Globally exponentially stable attitude and gyro bias estimation with application to GNSSINS integration," *Automatica*, vol. 51, DOI 10.1016/j.automatica.2014.10.076, pp. 158–166, Jan. 2015.
- [14] D. E. Zlotnik and J. R. Forbes, "Exponential convergence of a nonlinear attitude estimator," *Automatica*, vol. 72, DOI 10.1016/j.automatica.2016.05.018, pp. 11–18, Oct. 2016.
- [15] D. E. Zlotnik and J. R. Forbes, "Higher Order Nonlinear Complementary Filtering on Lie Groups," *IEEE Transactions on Automatic Control*, vol. 64, DOI 10.1109/TAC.2018.2845681, no. 5, pp. 1772–1783, May. 2019.
- [16] A. Astolfi and R. Ortega, "Immersion and invariance: a new tool for stabilization and adaptive control of nonlinear systems," *IEEE Trans*actions on Automatic Control, vol. 48, DOI 10.1109/TAC.2003.809820, no. 4, pp. 590–606, Apr. 2003.
- [17] A. Astolfi, D. Karagiannis, and R. Ortega, Nonlinear and Adaptive Control with Applications, ser. Communications and Control Engineering. London: Springer London, 2008.
- [18] B. Zhao, B. Xian, Y. Zhang, and X. Zhang, "Nonlinear Robust Adaptive Tracking Control of a Quadrotor UAV Via Immersion and Invariance Methodology," *IEEE Transactions on Industrial Electronics*, vol. 62, DOI 10.1109/TIE.2014.2364982, no. 5, pp. 2891–2902, May. 2015.
- [19] Z.-E. Lou and J. Zhao, "Immersion- and invariance-based adaptive stabilization of switched nonlinear systems," *International Journal of Robust and Nonlinear Control*, vol. 28, DOI 10.1002/rnc.3864, no. 1, pp. 197–212, Jan. 2018.
- [20] J. Keighobadi, M. Hosseini-Pishrobat, J. Faraji, A. Oveisi, and T. Nestorović, "Robust nonlinear control of atomic force microscope via immersion and invariance," *International Journal of Robust and Nonlinear Control*, vol. 29, DOI 10.1002/rnc.4421, no. 4, pp. 1031– 1050, 2019.
- [21] D. Karagiannis, D. Carnevale, and A. Astolfi, "Invariant Manifold Based Reduced-Order Observer Design for Nonlinear Systems," *IEEE Trans*-

- actions on Automatic Control, vol. 53, DOI 10.1109/TAC.2008.2007045, no. 11, pp. 2602–2614, Dec. 2008.
- [22] A. Astolfi, R. Ortega, and A. Venkatraman, "A globally exponentially convergent immersion and invariance speed observer for mechanical systems with non-holonomic constraints," *Automatica*, vol. 46, DOI 10.1016/j.automatica.2009.10.027, no. 1, pp. 182–189, Jan. 2010.
- [23] M. Tavan, A. Khaki-Sedigh, M.-R. Arvan, and A.-R. Vali, "Immersion and invariance adaptive velocity observer for a class of Euler-Lagrange mechanical systems," *Nonlinear Dynamics*, vol. 85, DOI 10.1007/s11071-016-2696-2, no. 1, pp. 425–437, Jul. 2016.
 [24] I. U. Khan, D. Wagg, and N. D. Sims, "Nonlinear robust observer design
- [24] I. U. Khan, D. Wagg, and N. D. Sims, "Nonlinear robust observer design using an invariant manifold approach," *Control Engineering Practice*, vol. 55, DOI 10.1016/j.conengprac.2016.06.015, pp. 69–79, Oct. 2016.
- [25] F. Morbidi, G. L. Mariottini, and D. Prattichizzo, "Observer design via Immersion and Invariance for vision-based leader-follower formation control," *Automatica*, vol. 46, DOI 10.1016/j.automatica.2009.10.016, no. 1, pp. 148–154, Jan. 2010.
- [26] C. Murguia, R. H. Fey, and H. Nijmeijer, "Immersion and invariance observers with time-delayed output measurements," *Communications in Nonlinear Science and Numerical Simulation*, vol. 30, DOI 10.1016/j.cnsns.2015.06.005, no. 1-3, pp. 227–235, Jan. 2016.
- [27] R. M. Murray, Z. Li, and S. Sastry, A mathematical introduction to robotic manipulation. Boca Raton: CRC Press, 1994.
- [28] H. Nourmohammadi and J. Keighobadi, "Fuzzy adaptive integration scheme for low-cost SINS/GPS navigation system," *Mechanical Systems* and Signal Processing, vol. 99, DOI 10.1016/j.ymssp.2017.06.030, pp. 434–449, Jan. 2018.
- [29] S. Ishijima and A. Kojima, "Practical Stabilization of Nonlinear Control Systems," *IFAC Proceedings Volumes*, vol. 25, DOI 10.1016/S1474-6670(17)49755-2, no. 21, pp. 216–219, Sep. 1992.
- [30] H. K. Khalil, Nonlinear control. Boston: Pearson, 2015.
- [31] J. Keighobadi, "Fuzzy calibration of a magnetic compass for vehicular applications," *Mechanical Systems and Signal Processing*, vol. 25, DOI 10.1016/j.ymssp.2010.11.005, no. 6, pp. 1973–1987, Aug. 2011.

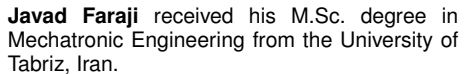


Jafar Keighobadi received the Ph.D. degrees in Mechanical Engineering and Control Systems from Department of Mechanical Engineering, Amirkabir University of Technology, Iran, in 2008.

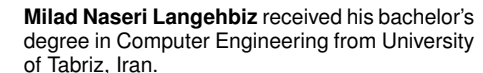
He is currently an Associate Professor of Mechanical Engineering Department at the University of Tabriz. His research interests include artificial intelligence, estimation and identification, nonlinear robust control, and GNC.



Since 2016, he has been a research assistant at the Faculty of Mechanical Engineering, the University of Tabriz. His research interests include nonlinear control, disturbance estimation-based control, and nonlinear observers.



Since 2014, he has been working toward the Ph.D. degree with the Department of Mechanical Engineering, the University of Tabriz. His research interests include integrated navigation systems, estimation and optimization theory, inertial and non-inertial sensors calibration.



He is currently pursuing his M.Sc. studies in Computer Science at Politecnico di Milano. His research interests include autonomous robots, positioning systems, and industrial IoT.



